Diffraction focusing of x rays

V. L. Indenbom

Institute of Crystallography, USSR Academy of Sciences, Moscow

E. V. Suvorov

Institute of Solid State Physics, USSR Academy of Sciences, Moscow

I. Sh. Slobodetskiĭ

Institute of High Pressure Physics, USSR Academy of Sciences, Moscow

(Submitted February 5, 1976)
Zh. Eksp. Teor. Fiz. **71**, 359–369 (July 1976)

A theoretical and experimental study is reported of the main factors governing the diffraction focusing of x rays, including the angular aperture, the spatial distribution, the spectral composition and coherence of the initial packet, the particular parameters and true quality of the crystal, and the properties of the interferometer cut from the crystal. By improving the system, it has been possible to achieve the sharp diffraction focusing (with micron precision) predicted previously {V.L. Indenbom, I.Sh. Slobodetskiĭ, and K.G. Truni, Zh. Eksp. Teor. Fiz. **66**, 1110 (1974) [Sov. Phys. JETP **39**, 542 (1974)]} and to test the various ways of using the effect in x-ray optical devices.

PACS numbers: 61.10.Dp, 61.10.Fr, 07.85.+n

Diffraction focusing of x rays resulting from their successive refraction in the plates of a two-crystal interferometer was predicted in a previous paper.[1] This phenomenon was later discovered experimentally.[2] Subsequent work[3,4] demonstrated the importance of diffraction focusing in the formation of the x-ray image of crystal-lattice defects.

The phenomenon of diffraction focusing is illustrated schematically in Fig. 1. When a narrow incident beam is diffracted in the first plate of a Π-shaped interferometer, the wave field fills the triangle lying between the directions of the transmitted and reflected waves, and a broader refracted beam leaves the plate (Fig. 1a). The beam doubles its width as a result of diffraction in the second plate, but the wave field in the doubly refracted beam is focused down to a high-intensity narrow peak at the center of the beam (Fig. 1b).

However, both the experiments described in[2] and those mentioned at the end of[1] showed that agreement with theoretical predictions was only qualitative. The sharpness of focusing was not as good as one would expect from the theory. The broadening of the image of the first slit amounted to some tens of microns instead of the predicted 1–2 μ. The central peak had a fine structure and was accompanied by satellites. As a result of the discrepancy between theory and experiment, the possible realization of the various practical applications of diffraction focusing noted in[1], and the development of x-ray optics devices with diffraction lenses, has remained an open question.

The present paper is concerned with the theoretical and experimental study of the main factors governing the diffraction focusing effect, including the spatial distribution, the angular aperture, the spectral composition and coherence of the initial wave packet, the particular parameters and true quality of crystals, and the properties of the interferometer as a whole. An interpretation is given of the structure of the doubly-diffracted beams in terms of the theory developed previously, and this is used to establish the conditions that are necessary for achieving the sharp diffraction focusing predicted in[1] and for the practical application of this effect with the theoretical (micron) diffraction broadening. The application of these results to the reconstruction and transfer of the x-ray image, the formation of a spatially modulated Borrmann wave field in highly absorbing crystals, and the development of various x-ray optics devices with diffraction lenses (high-resolution x-ray spectrometer, high-luminosity achromatic diffraction lens, and so on) are described in special publications.[5–7]

1. ANALYSIS OF FACTORS GOVERNING DIFFRACTION FOCUSING

The ideal case, where a monochromatic wave $E_0(x, z)$ is incident on the surface $z = 0$ of the first plate of the Laue-type interferometer after passing through a narrow slit, was discussed in[1]. The wave field $E_1(x, z)$ diffracted by the first plate is given in this case by the Riemann function[8,9]

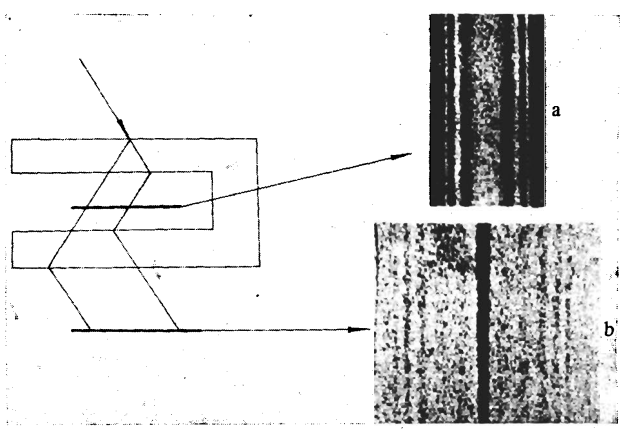

FIG. 1. Diffraction focusing of x rays in the Π-interferometer: a—image of slit after first plate [Eq. (2)]; b—transformation of this image in the second plate [see Eqs. (4) and (5)].

$$G(x,z,\beta)=\frac{1}{2}\exp\left[-i\beta\frac{\pi}{\Lambda}(z-x\operatorname{ctg}\vartheta)\right]\theta(z-|x|\operatorname{ctg}\vartheta)$$
$$\times J_0\left(\frac{\pi}{\Lambda}(z^2-x^2\operatorname{ctg}^2\vartheta)^{1/2}\right), \quad (1)$$

and, in particular, when $E_0(x,0)=\delta(x)$,

$$E_1(x,z,\beta)=i\Delta^{-1}G(x,z,\beta). \quad (2)$$

In these expressions, $\theta(x)$ is the unit step function, $J_0(x)$ is the Bessel function of order zero, ϑ is the Bragg angle, $\Lambda=(\lambda\cos\vartheta)/|\chi|$ is the extinction length corresponding to the splitting of the dispersion surface on the boundary of the Brillouin zone, λ is the wavelength, χ is the effective Fourier component (taking into account the polarization factor) of the polarizability of the crystal for the given reflection vector, $\Delta=(\Lambda/\pi)\tan\vartheta$, and β is the parameter representing the departure from the Bragg condition. In particular, a small change φ in the Bragg angle corresponds to

$$\beta=\frac{2\Lambda}{\lambda}\varphi\sin\vartheta=\frac{\Lambda}{d}\varphi, \quad (3)$$

where d is the reflecting-plane separation for the given reflection. In contrast to[1] we have confined our attention to the centrally symmetric crystal, and have written our equations in a natural coordinate frame in which the z and x axes lie in the plane of scattering along the intersection with the reflecting plane and along the normal to it, respectively.

The structure of the doubly-diffracted beam E_{01} after the interferometer is given by the convolution[1]

$$E_{01}(x,z,\beta)=-\Delta^{-2}G(x,z_1,\beta)*G(x,z_2,\beta)$$
$$=-\frac{1}{4\Delta^2}\operatorname{tg}\vartheta\exp\left[-i\beta\frac{\pi}{\Lambda}(Z-x\operatorname{ctg}\vartheta)\right]\theta(Z-|x|\operatorname{ctg}\vartheta)$$
$$\times\int_z^Z J_0\left(\frac{\pi}{\Lambda}(t^2-x^2\operatorname{ctg}^2\vartheta)^{1/2}\right)dt, \quad (4)$$

where z_1 and z_2 are the thicknesses of the first and second plates of the interferometer, respectively, $Z=z_1+z_2$ is the total thickness of the plates, $\gamma=\max(|x|\cot\vartheta,|\delta|)$, and $\delta=z_2-z_1$ is the thickness difference.

For an interferometer with sufficiently thick plates ($Z\gg\Lambda$) with roughly equal arms ($\delta\ll\Lambda$), the wave field in the central part of the beam can be written in the form

$$E_{01}(x,Z,\beta)=-\frac{1}{4\Delta}\exp\left[-i\beta\frac{\pi}{\Lambda}(Z-x\operatorname{ctg}\vartheta)\right]$$
$$\times\theta(Z-|x|\operatorname{ctg}\vartheta)\left\{e^{-|x|/\Delta}+J_1\left(\frac{\pi}{\Lambda}(Z^2-x^2\operatorname{ctg}^2\vartheta)^{1/2}\right)\right.$$
$$\left.-\frac{\pi}{\Lambda}\theta(|\delta|-|x|\operatorname{ctg}\vartheta)\int_{|x|\operatorname{ctg}\vartheta}^{|\delta|}J_0\left(\frac{\pi}{\Lambda}(t^2-x^2\operatorname{ctg}^2\vartheta)^{1/2}\right)dt\right., \quad (5)$$

where $J_1(x)$ is the Bessel function of order one.

The first term in (5) describes the sharp peak at the center of the image with half-width $\Delta\ln 2$ which, in the case of Mo$K\alpha$ radiation and the (111) reflections from silicon [subsequently denoted by Si(111)Mo$K\alpha$], amounts to 1 μ whereas, for the Si(220)Mo$K\alpha$ and Si(224)Mo$K\alpha$ reflections, this figure amounts to 1.4 and 3.5 μ, respectively. The second term in (5) determines the shape of the broad pedestal on which the central peak is located in the equal-arm interferometer. The third term describes the contribution of the thickness difference and turns out to be very important in practice. Whilst in the equal-arm interferometer ($\delta=0$) the intensity of the central peak for $Z>10\Lambda$ exceeds the background intensity by a factor of 1.5–2 according to[1], the intensity of the central peak is substantially reduced and the peak itself is split for a thickness difference smaller by an order of magnitude than Λ, and its total area in the imaging function (5) is reduced in proportion to $\cos(\pi\delta/\Lambda)$, so that the intensity is reduced by a factor of four when $|\delta|=\Lambda/3$, and becomes zero for $|\delta|=\Lambda/2$. Moreover, the condition $|\delta/\Lambda|<0.1$ correspond to very stringent tolerances in the fabrication of the interferometer [for the Si(220)Mo$K\alpha$ or Si(224)Mo$K\alpha$ reflections, the thickness difference must be less than 3.5–4 μ].

The situation becomes much more complicated when the actual experimental conditions are taken into account. Thus, the entrance slit has a finite width so that the imaging function (4) must be integrated over the width of the slit, taking into account the angular and spectral compositions of the incident wave packet. A problem of this kind has already been solved in[8,10] but only in the approximation involving a perfectly monochromatic incident wave. In our case, integration of the imaging function given by (4) and (5) for each monochromatic wave and a slit of width $2a>\Delta$ leads to the spreading of the image by an amount of the order of the diffraction broadening Δ, and to a reduction in the height of the central peak by the factor

$$f(\beta)=a^{-1}\int_0^a dx\,e^{-x/\Delta}\cos\frac{\beta x}{\Delta}=\frac{\Delta}{a(1+\beta^2)}\left[1-e^{-a/\Delta}\left(\cos\frac{\beta a}{\Delta}-\beta\sin\frac{\beta a}{\Delta}\right)\right]. \quad (6)$$

We note that the interferometer is assumed to have equal arms and that the shape of the pedestal undergoes only a slight change over distances of the order of a.

For a narrow collimated incident beam ($\beta\ll 1$), the reduction in the image intensity contrast is determined by the coefficient

$$f(0)^2=\{(\Delta/a)[1-e^{-a/\Delta}]\}^2,$$

which is equal to 0.16 for $a=5$ μ in the case of Si(220)Mo$K\alpha$ reflections, and 0.40 in the case of the Si(224)Mo$K\alpha$ reflections. An increase in the aperture of the system is accompanied by an increase in the contribution of deflected beams with $\beta\neq 0$, and there is a simultaneous reduction both in the height of the peak [in accordance with (6)] and in the background level [because of the phase factor $\exp(i\beta x/\Delta$ in the imaging function]. Conventional two-slit collimators transmit beams for which the parameter β assumes values up to a few units ($\beta=1$ corresponds to the angular width of the dynamic maximum). Summation of the contributions of all the beams in a broad angular interval up to $|\beta|\gg 1$ is equivalent, according to the Parseval formula, to the following approximate expression for the contrast reduction coefficient:

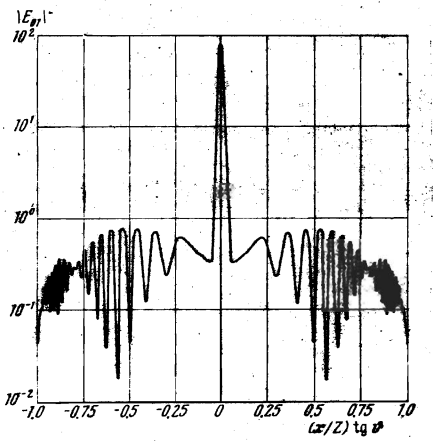

FIG. 2. Calculated image of the slit in the doubly diffracted beam [slit width 10 μ, $z_1 = z_2 = 0.45$ mm, Si(224)Mo$K\alpha$].

$$\frac{a}{\pi\Delta}\int_{-\infty}^{\infty}|f(\beta)|^2 d\beta = a^{-1}\int_0^a e^{-2x/\Delta}\,dx = \frac{\Delta}{2a}\left[1-e^{-2a/\Delta}\right], \qquad (6')$$

which, for $a = 5$ μ, corresponds to a reduction in contrast down to 0.4 and 0.87 for the Si(220)Mo$K\alpha$ and Si(224)Mo$K\alpha$ reflections, respectively. Thus, as in the case of narrow beams, the use of the (224) reflections is advantageous for broad beams if higher intensity contrast is to be achieved even though some loss of resolution is then introduced because the diffraction broadening in the case of the (224) reflection is substantially greater than for the (220) reflection.

As an illustration, Fig. 2 shows, on a semilogarithmic scale, the calculated image of a 10-μ slit in an equal-arm interferometer consisting of silicon plates with $z_1 = z_2 = 0.45$ mm in the case of Si(224)Mo$K\alpha$. It was assumed in the calculation that the beam incident on the crystal was highly collimated, monochromatic, and unpolarized. For waves with different polarizations, the Fourier components of the crystal polarizability (and, correspondingly, the extinction lengths and arguments of the imaging functions) differ by the factor $\cos 2\vartheta \approx 0.8$. The result of this is that, when slit images corresponding to waves with different polarizations are superimposed, the intensity oscillations do not reach the zero level. In accordance with the theory, the half-width of the peak at the center of the image is 13.5 μ and its amplitude exceeds the background by a factor of two.

The fact that the incident radiation is not monochromatic can be taken into account by allowing for the difference between the Bragg angles and, consequently, between the parameters β for the different monochromatic waves. If we combine the Bragg conditions with (3), we obtain the linear function

$$\beta = (\Delta\lambda/\delta\lambda)\,(\Delta/l_0)\sin\vartheta, \qquad (3')$$

where $\Delta\lambda$ is measured from the wavelength corresponding to the situation where the Bragg-Vul'f conditions are strictly satisfied, $\delta\lambda$ is the natural width of the spectral line used in the experiment, and $l_0 = \lambda^2/2\pi\delta\lambda$ is the corresponding train length (coherence length) of the x-ray radiation. The section through the wave train by the critical surface whose length is $l = l_0 \operatorname{cosec}\vartheta$ is always small in comparison with Δ [for the Mo$K\alpha$ radiation, we have $\delta\lambda \approx (0.24\times 0.27)\times 10^{-11}$ cm and $l_0 \approx 3\times 10^{-6}$ cm, which is lower by two orders of magnitude than the diffraction broadening Δ]. Thus, the elementary wave trains successively scan the slit with coherently illuminated strips of width l which, according to (3'), is small in comparison with the details of the imaging function for all beams with $|\beta|$ up to 10 or more, so that the fact that the radiation is not monochromatic does not, within the limits of the natural linewidth, smear out the details of the image.[1)]

When the geometry of the system is such that the beam centers do not coincide for different wavelengths, the effect of the fact that the incident radiation is not monochromatic is generally different. It produces appreciable chromatic aberration which can be taken into account by considering the diffraction of each monochromatic wave independently and adding up the intensities of the individual monochromatic image components. Estimates of the linear dispersion of the system based on the Bragg-Vul'f formula shows that the inclusion of chromatic aberration leads to a broadening of the image by an amount given by

$$\delta x = \frac{D}{\lambda}\frac{\sin\vartheta}{\cos^3\vartheta}\Delta\lambda,$$

where D is of the order of the distance between the slit and the photographic plate (rigorous calculations show that D corresponds to this distance minus the thickness of the interferometer plates and twice the gap between the plates[6,7]). Unless special measures are taken, chromatic broadening of the image in systems of the usual size may amount to some tens of microns and may mask the focusing effect.[7] It is precisely this effect that prevented satisfactory focusing in the experiments listed at the end of[1].

Chromatic aberration cannot, however, explain the results published in[2], where a microfocus tube and a 10-μ slit were employed. These experiments show the presence of not only a broadening of the central peak up to 20 μ, but also of broad satellites which merge with the main peak and broaden the slit image up to 50–70 μ, which in no way corresponds to the angular and spectral composition of the beam. The large-scale oscillations in image intensity seen in Fig. 2 may be connected with the second term in (5), which gives rise to oscillations with a period of the order of $(Z\Lambda)^{1/2}\cot\vartheta$, which, under the conditions of the experiments described in[2], corresponds to approximately 70 μ [Si(224)Mo $K\alpha$ reflection, $\Lambda = 42$ μ, $Z = 0.9$ mm, $\vartheta = 18.5°$]. Using the well-known asymptotic properties of Bessel functions for large values of the argument to estimate the height of these oscillations, we can readily verify that, for the oscillations to appear, we would require a reduction in the height of the central peak by roughly an order of magnitude, which cannot be ensured for reasonable values of the above parameters.

The only remaining possibility is that the structure of

the doubly diffracted beams observed experimentally is determined by imperfections in the crystals used. We note, to begin with, that the estimates given above were obtained for perfect nonabsorbing crystals. Let us therefore begin by estimating the absorption of x rays in the interferometer components. To do this, we must multiply the imaging function (5) by the factor $k = \exp(-\mu Z/2)$, where μ is the photoelectric absorption coefficient, and replace the real parameter Λ by its complex analog $\Lambda = \Lambda' + i\Lambda''$, which represents the fact that the Fourier components of the crystal polarizability are complex (see, for example, [5]).

According to (5), the ratio of the background to central-peak intensities for an equal-arm interferometer is equal to the square of the modulus of the Bessel function $J_1(\pi Z/\Lambda)$ of the complex argument $\pi Z/\Lambda = (\pi Z/|\Lambda|^2)(\Lambda - i\Lambda'')$:

$$\left|J_1\left(\frac{\pi}{\Lambda}Z\right)\right|^2 \approx \frac{2\Lambda}{\pi^2 Z}\left[\operatorname{ch}\frac{2Z\Lambda''}{|\Lambda|^2} - \sin\frac{2\pi Z\Lambda'}{|\Lambda|^2}\right].$$

As Z increases, this ratio oscillates with a period approaching $|\Lambda|$, and an amplitude $2|\Lambda|/\pi^2 Z$, about the smooth curve $(2|\Lambda|/\pi^2 Z)\cosh(2Z\Lambda''/|\Lambda|^2)$, which has a shallow minimum near $Z \approx 0.6|\Lambda|^2/\Lambda''$ that approximately corresponds to $\mu Z = 1.2$ since, for silicon, $2\Lambda''/|\Lambda|^2 \approx \mu$. In[2], we use $\mu Z \approx 1.3$ and $Z/|\Lambda| \approx 22$, so that absorption reduces the difference between the peak and the background by roughly a factor of 1.5, but cannot ensure the appearance of high satellites. Absorption can lead to complete redistribution of the wave field in interferometers with highly absorbing components,[5] but does not alter the general structure of the beam in the case of the more usual, weakly absorbing plates.

Another characteristic feature of crystals actually used in practice is disorientation. Although the interferometer is usually cut from a single crystal, and this is done so as to retain the stiffness of the structure, the interferometer arms may turn out to be slightly misaligned because of disorientation or variations in the lattice parameter in the original crystal.

Even when dislocation-free crystals are used, one frequently observed relative deformations and disorientations of $\sim 10^{-7}$ which, according to (3), corresponds to a difference in the values of β for the two arms of the interferometer amounting to ~ 0.01.

In order to take the disorientation effect into account, we must replace the convolution given by (4) by the convolution of the Riemann functions (1) with different values not only of z but also of β, i.e.,

$$G(x, z_1, \beta_1) * G(x, z_2, \beta_2),$$

so that, when we go on to the convolution of the Fourier transforms of the Riemann functions, this reduces to a consideration of the integral

$$I = \int_{-\infty}^{\infty} \frac{d\omega}{\Omega_1\Omega_2} \sin\frac{\pi\Omega_1 z_1}{\Lambda} \sin\frac{\pi\Omega_2 z_2}{\Lambda} e^{i\omega x/\Lambda}, \qquad (7)$$

$$\Omega_i = (1+(\omega-\beta_i)^2)^{1/2}.$$

To within the above phase factor in the function I, which we have already investigated, let us set $\beta_1 = -\beta_2 = \beta$, express z_1 and z_2 in terms of the half sum and half difference of these quantities, and separate out the slowly varying terms in the integrand (β and δ are small), which provide the main contribution to the integral and correspond to the factor

$$\cos\left[\frac{\pi}{\Lambda}(\Omega_1 z_1 - \Omega_2 z_2)\right] \approx \cos\left[\frac{\pi}{\Lambda}\left(\frac{\beta\omega Z}{\Omega} + \Omega\delta\right)\right], \quad \Omega = (1+\omega^2)^{1/2}. \qquad (8)$$

Replacing Ω_i by Ω in the denominator of the integrand in (7), and substituting $\omega = \tan\psi$, we obtain

$$I = \int_0^{\pi/2} d\psi \cos\frac{x\operatorname{tg}\psi}{\Delta} \cos\left(\frac{\pi}{\Lambda}\beta Z\sin\psi + \frac{\pi}{\Lambda}\delta\sec\psi\right). \qquad (9)$$

When $\beta = 0$, the result given by (4) follows from (7). When $\delta = 0$ and $x = 0$, the expression given by (9) becomes

$$I = {}^1/_2\pi J_0(\pi Z\beta/\Lambda), \qquad (10)$$

and, hence, it follows that the height of the central peak in the imaging function undergoes sharp (down to zero) oscillations when the disorientation β changes by an amount of the order of Λ/Z, which corresponds to a change in the Bragg angle by a hundredth of a second under the conditions prevailing in the experiments described in[2].

Disorientation of the interferometer plates also gives rise to the appearance of oscillations on the peak profile. Thus, when $\delta = 0$ and x is small, we can obtain an estimate for the integral in (9) by replacing $\tan\psi$ by ψ or $\sin\psi$, which reduces the integral to the sum of Anger functions or Bessel functions, respectively, with an oscillatory dependence on both β and x.

The sensitivity of the image to the disorientation of the interferometer plates is reduced somewhat by the thickness-difference effect. Since the disorientation β is present in (9) in the form a linear combiantion with δ, it is clear that the contribution of one of the effects may, to some extent, be compensated by the second. It is readily seen, in particular, that when $\delta/\Lambda \gtrsim \beta Z$, the argument of the second cosine in (9) remains small within a considerable range of variation of ψ, so that most of the height of the central peak is retained. In relation to the experiments described in[2], the above condition corresponds to an increase in the thickness difference by a few microns in order to compensate a disorientation of the plates of the order of a hundredth of a second of arc.

The above approximate estimates have been improved and augmented by quantitative evaluations of the convolution (7) performed with the aid of a computer for the characteristic values of the parameters of the problem (Fig. 3). Curve 1 describes the shape of the peak for an equal-arm interferometer ($z_1 = z_2 = 13\Lambda$) in the absence of disorientation. As the disorientation increases up to $\beta = 0.029$, which corresponds to the zero of the Bessel function in (10), the peak height is, in fact, found to fall to zero and the satellites appear (curve 2). When $\beta = 0.089$, which corresponds to the second maximum on

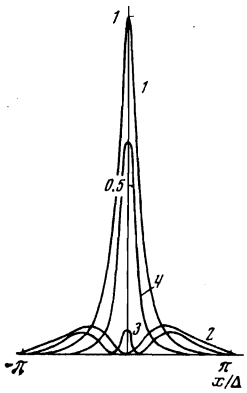

FIG. 3. Effect of thickness difference and disorientation of interferometer plates on the shape of the central peak on the imaging function: 1—$\delta = 0$, $\beta = 0$; 2—$\delta = 0$, $\beta = 0.029$; 3—$\delta = 0$, $\beta = 0.089$; 4—$\delta = 0.01Z$, $\beta = 0.029$. The other parameters are the same as in Fig. 2. The peak intensity corresponding to (1) was taken as the unit intensity.

the Bessel function in (10), the central peak reappears (curve 3). Compensation of the effect of disorientation $\beta = 0.029$ is achieved for a thickness difference $\delta = 0.005\Lambda \approx 0.01Z$ (curve 4). In the case of the Si, MO$K\alpha$ reflections, the above parameters correspond to disorientations of 0.04" and 0.1" for the (220) reflection and 0.016" and 0.05" for the (224) reflection when $\delta \approx 9\ \mu$.

2. EXPERIMENTAL STUDY OF THE SPATIAL STRUCTURE OF THE IMAGE

As theoretical estimates of the effect of the various factors on image structure and the quality of diffraction focusing became available, a comparison was carried out between theory and experiment and, on this basis, the design of the interferometers was improved. In all the experiments, we used interferometers consisting of silicon plates with $z_1 = z_2 = 0.45$ mm, i.e., sufficiently thick in comparison with the extinction length [$Z/\Lambda \approx 25$ for the (220) reflection and $Z/\Lambda \approx 21$ for the (224) reflection in the case of the Mo$K\alpha$ radiation], and at the same time, sufficiently thin ($\mu Z \approx 1.3$) to ensure that absorption could not suppress the central peak relative to the background. The experiments were performed with the D-4C and RU-3HM instruments, using the A-3 cameras manufactured by Rigaky Denky and Mo$K\alpha$ radiation. The size of the projected focal spot in the direction of the reflection vector was 3–5 μ. The shaping slit was 10 μ wide in all the experiments. The image was recorded photographically on MK plates. The Carl Zeiss G-II microdensitometer was used to record the intensity-distribution curves. For quantitative intensity measurements, we used negatives on which the degree of blackness lay within the linear range of the characteristics curve of the MK photographic plate.

In the initial experiments, we tried to obtain maximum diffraction focusing by confining our attention to the (220) reflection for which the calculated diffraction broadening amounted to 1.4 μ. However, in practice, similar results could be obtained with the more convenient (224) reflection corresponding to a diffraction broadening of ~ 3.5 μ.

When it was established that the diffraction broadening effect was masked by the more substantial contribution of the plate thickness difference and the nonmonochromatic character of the radiation, we concentrated out attention on the (224) reflection for which the tolerance on the thickness difference δ and incident-beam collimation was less stringent, and the intensity of the diffracted beam—especially the central peak—was greater, so that a considerable economy could be effected in the exposure time.

To investigate the effect of the thickness difference, we constructed interferometers with wedge-shaped plates such that the diffraction vector was perpendicular to the wedge generator and each section through the interferometer by the scattering plane corresponded to a definite value of the thickness difference. Figure 4 demonstrates the focusing effect in one such interferometer. As one departs from the section corresponding to equal plate thicknesses, the slit image gradually broadens and splits. Figure 4 shows micrographs for the section with equal plate thickness, and for two sections a few millimeters away from this section. The complicated structure of the image corresponds, according to Fig. 3, to an appreciable contribution of the disorientation of the plates. The fact that the theoretical estimates of the influence of the disorientation effect were valid was verified by examining an interferometer with a dislocation. Band splitting of the kind shown in Fig. 4 was found to begin at a distance of 1 mm from the dislocation, which corresponded to a rotation of the lattice through an angle of 0.02".

Figure 5 shows photographs and micrographs of the E_{11}, E_{10}, and E_{01} beams for one of the successful specimens. The image width is 12 μ for the doubly diffracted beam, and 15 μ for the E_{11} and E_{10} beams, i.e., once reflected (in the first and second arms, respectively) and once transmitted. The overall spatial intensity distribution is in good agreement with the theory for all three beams.[2] The broadening in the E_{10} and E_{11} beams is up to 5 μ (calculated broadening 3.5 μ), and the broadening in the doubly diffracted beam is 2 μ. Figures 5a–5c show that the intensities of the central peak are not appreciably different, which leads to an interesting estimate for the upper limit of the coherence length of the x rays. We note that the central peak on the imaging function for the E_{10} and E_{11} beams consists

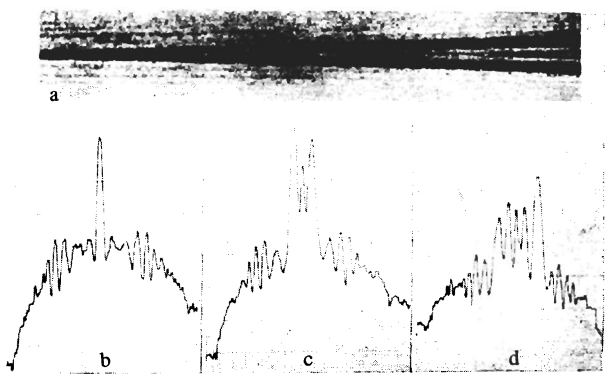

FIG. 4. Image of slit in doubly diffracted beam obtained in interferometer with wedge-shaped plate [slit width 10μ, Si(224)Mo$K\alpha$]; a—general appearance of the central part of the topogram; b—micrograph for equal-thickness section; c and d—ditto for sections at 7 and 14 mm from the equal-thickness position.

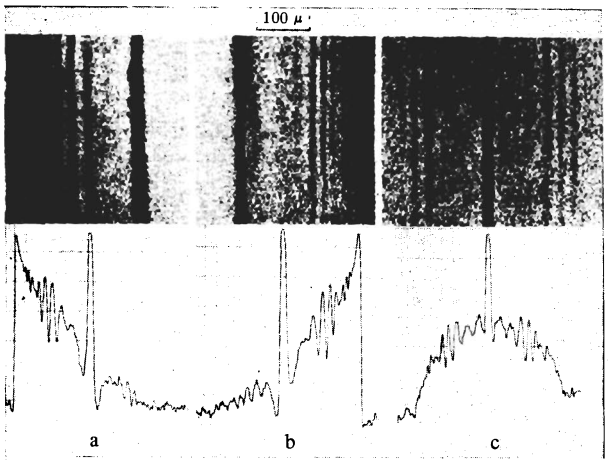

FIG. 5. Image of slit and corresponding micrographs for the E_{11} (a), E_{10} (b), and E_{01} (c) beams in the case of the equal-thickness interferometer [$\delta < 2\mu$, slit width 10μ, Si(224) Mo$K\alpha$].

of two antisymmetric peaks of the form $(x/|x|) \times \exp(-|x|/\Delta)$, according to[11]. Averaging of the imaging function over the coherence length $l = l_0 \operatorname{cosec}\vartheta$ of the wavefront in the case of narrow collimation is admissible only provided[2)] that $l \ll \Delta$. Hence, it follows that, in our case, $l_0 \ll 0.4$–$1.5\ \mu$, where the first figure is given for the (220) reflection and the second for the (224) reflection, whereas the estimated l_0 based on the spectral width of the Mo$K\alpha_1$ line[11] yields $l_0 \sim 0.3 \times 10^{-5}$ cm.

Initially, the interferometer design was such that the geometry of the inner surface of the plates could not be controlled. To ensure reliable control of the thickness difference, we made Π-shaped interferometers with a large gap between the plates. The thickness difference was then reduced to 1–2 μ. It was much more difficult to reduce the disorientation of the plates. An increase in the stiffness of the system did not in itself resolve the difficulty, and higher quality dislocation-free crystals had to be used, so that a search had to be carried out for specimens with weakly defined growth zones, i.e., the plates had to be chosen by trial and error.

In several cases, the diffraction broadening was almost in agreement with the calculations. The intensity ratio for the image and background was, in the best cases, 30–40 instead of the figure of 100 in Fig. 2. This difference was due either to slight disorientation of the plates (one-hundredth of a second of arc was enough), or a slight spreading of the wave packet in the gap between the plates. Independently of the solution of this difficult problem, the diffraction focusing achieved in our work enables us to proceed to a practical realization of the new x-ray optics devices proposed in[1]. In particular, a spectrometer with the diffraction lens[6] has already been tested, and a high-luminosity achromatic lens has been developed. The first experiment on the transmission of an x-ray image has been carried out.[7] Moreover, further studies of the effects associated with finite x-ray coherence lengths has been carried out.[12]

The authors are greatly indebted to V. I. Nikitenko for his constant interest in this research and active assistance in the experiments, Yu. M. Kagan' and V. I. Ivernova for useful discussions of the results, and A. M. Arustamyan for control calculations based on theoretical estimates of the influence of absorption and disorientation on the focusing effect.

1)The same conclusion can be obtained directly by considering the contribution of the monochromatic waves forming the wave train. A similar device enables us to take into account the angular divergence of the primary beam (spherical aberration), which results in a certain compression of the wave packet (Kato focusing) at the entrance surface which does not result in considerable distortion of the focusing effect.

2)The same result follows from the estimate given by (3′) for the spectral interval which includes, for narrow collimation, waves with $|\beta| \sim 1$ that are necessary to achieve high intensity of the image at the center of the E_{10} and E_{11} beams.

[1]V. L. Indenbom, I. Sh. Slobodetskiĭ, and K. G. Truni, Zh. Eksp. Teor. Fiz. **66**, 1110 (1974) [Sov. Phys. JETP **39**, 542 (1974)].
[2]É. V. Suvorov and V. I. Polovinkina, Pis'ma Zh. Eksp. Teor. Fiz. **20**, 326 (1974) [JETP Lett. 20, 145 (1974)].
[3]E. V. Suvorov, V. I. Polovinkina, V. I. Nikitenko, and V. L. Indenbom, Phys. Status Solidi A **26**, 385 (1974).
[4]V. L. Indenbom and I. Sh. Slobodetsky, Phys. Status Solidi B **71**, 751 (1975).
[5]V. L. Indenbom and I. Sh. Slobodetsky, Phys. Status Solidi B **73**, K9 (1976).
[6]V. L. Indenbom and É. V. Suvorov, Pis'ma Zh. Eksp. Teor. Fiz. **23**, 485 (1976) [JETP Lett. **23**, 441 (1976)].
[7]V. L. Indenbom and A. G. Aladzhadzhyan, Dokl. Akad. Nauk SSSR **227**, 827 (1976) [Sov. Phys. Dokl. 21, 191 (1976)].
[8]I. Sh. Slobodetskiĭ, F. N. Chukhovskiĭ, and V. L. Indenbom, Pis'ma Zh. Eksp. Teor. Fiz. **8**, 90 (1968) [JETP Lett. **8**, 55 (1968)].
[9]A. Authier and D. Simon, Acta Crystallogr. Sec. A **24**, 527 (1968).
[10]I. Sh. Slobodetskiĭ and F. N. Chukhovskiĭ, Kristallografiya **15**, 1101 (1970) [Sov. Phys. Crystallogr. **15**, 953 (1971)].
[11]G. Brogren, Ark. Fys. **8**, 391 (1954); L. G. Paratt, Rev. Mod. Phys. **31**, 616 (1959).
[12]V. L. Indenbom, Kristallografiya 21, 479 (1976). [Sov. Phys. Crystallogr. **21**, 764 (1976)].

Translated by S. Chomet